

A homogenous solid polymer electrolyte prepared by facile spray drying method is used for room-temperature solid lithium metal batteries

Zehao Zhou^{1,§}, Tong Sun^{3,§}, Jin Cui¹, Xiu Shen², Chuan Shi¹ (✉), Shuang Cao³, and Jinbao Zhao² (✉)

¹ College of Physics, Qingdao University, Qingdao 266071, China

² Collaborative Innovation Center of Chemistry for Energy Materials, State Key Lab of Physical Chemistry of Solid Surfaces, State-Province Joint Engineering Laboratory of Power Source Technology for New Energy Vehicle, Engineering Research Center of Electrochemical Technology, Ministry of Education, College of Chemistry and Chemical Engineering, Xiamen University, Xiamen 361005, China

³ College of Chemistry and Chemical Engineering, Qingdao University, Qingdao 266071, China

[§]Zehao Zhou and Tong Sun contributed equally to this work.

© Tsinghua University Press and Springer-Verlag GmbH Germany, part of Springer Nature 2021

Received: 13 April 2021 / Revised: 6 June 2021 / Accepted: 16 June 2021

ABSTRACT

The aggregation of inorganic particles with high mass ratio will form a heterogeneous electric field in the solid polymer electrolytes (SPEs), which is difficult to be compatible with lithium anode, leading to inadequate ionic conductivity. Herein, a facile spray drying method is adopted to increase the mass ratio of inorganic particles and solve the aggregation problems of fillers simultaneously. The polyvinylidene fluoride (PVDF) with lithium bis(trifluoromethanesulfonyl)imide (LiTFSI) covers the surface of each $\text{Li}_{6.4}\text{La}_3\text{Zr}_{1.4}\text{Ta}_{0.6}\text{O}_{12}$ (LLZTO) granules during the nebulization process, then forming flat solid electrolytes via layer-by-layer deposition. Characterized by the atomic force microscope, the obtained solid electrolytes achieve a homogenous dispersion of Young's modulus and surface electric field. As a result, the as-prepared SPEs present high tensile strength of 7.1 MPa, high ionic conductivity of $1.86 \times 10^{-4} \text{ S}\cdot\text{cm}^{-1}$ at room temperature, and wide electrochemical window up to 5.0 V, demonstrating increased mechanical strength and uniform lithium-ion migration channels for SPEs. Thanks to the as-prepared SPEs, the lithium-symmetrical cells show a highly stable Li plating/stripping cycling for over 1,000 h at $0.1 \text{ mA}\cdot\text{cm}^{-2}$. The corresponding Li/LCoO₂ batteries also present good rate capability and excellent cyclic performance with capacity retention of 80% after 100 cycles at room temperature.

KEYWORDS

solid polymer electrolytes, spray drying, homogenous dispersion, solid lithium batteries, polyvinylidene fluoride/ $\text{Li}_{6.4}\text{La}_3\text{Zr}_{1.4}\text{Ta}_{0.6}\text{O}_{12}$ (PVDF/LLZTO), surface electric field

1 Introduction

The capacity limitation and security threats of liquid batteries hinder the development of electric vehicles (EVs) and the storage of the new energy in a smart grid [1–4]. The solid lithium metal batteries (SLBs) exhibit great potential in breaking through the aforementioned restrictions since the solid-state electrolytes (SSEs) enable the use of both the Li metal anodes and high-voltage cathodes [5, 6]. However, it is still a critical challenge to suppress the formation and growth of dendrite during the repetitive deposition and stripping processes [7–9].

The solid-state electrolytes include solid ceramic electrolytes (SCEs) and solid polymer electrolytes (SPEs) [10]. As the vital component of solid lithium batteries, SSEs receive growing attention [6, 11, 12]. The SCEs with high modulus and high Li⁺ transference number are regarded as the promising candidate to prevent lithium dendrites growth [13–15]. But Han et al. have proved that lithium dendrites nucleated in the SCEs, including the most promising $\text{Li}_2\text{S}-\text{P}_2\text{S}_5$ sulfide electrolyte and $\text{Li}_7\text{La}_3\text{Zr}_2\text{O}_{12}$ (LLZO) oxide electrolyte, because of their relatively high electronic

conductivity, which hinders their practical applications [16]. Compared with SCEs, the SPEs with a combination of polymer and Li salt show excellent flexibility. But low ionic conductivity of SPEs induces the formation and growth of Li dendrite and finally causes the short-circuit of cells. Optimized by adding nano-ceramic fillers, such as SiO_2 , Al_2O_3 , $\text{Li}_{0.35}\text{La}_{0.55}\text{TiO}_3$ (LLTO), and $\text{Li}_{6.4}\text{La}_3\text{Zr}_2\text{Al}_{0.2}\text{O}_{12}$ (LLZAO), the synthesized SPEs have improved significantly in both mechanical strength and ionic conductivity, which can block the Li dendrite and delay the fading of the cells [17–24]. However, the amount of ceramic fillers in polymer is limited to only ~ 10 wt.%–20 wt.% via simple combinations because of their huge difference in surface energy. Therefore, high mass ratio of fillers will promote the particles to aggregate, especially during the solvent volatilization process [25]. Unfortunately, the formation of Li dendrites resulted from the uniformity of the electric field and the ionic conductivity is limited concomitantly [25, 26].

How to avoid the agglomeration of ceramic filler is a key issue for further improvement of the ionic conductivity and delaying

Address correspondence to Chuan Shi, chuanshi@qdu.edu.cn; Jinbao Zhao, jbzhao@xmu.edu.cn

the growth of Li dendrite. Lin et al. prepared a solid polymer electrolyte with *in situ* hydrolysis of tetraethyl orthosilicate (TEOS) in the poly(ethyleneoxide) (PEO) solution, which showed increased electrochemical stability and ionic conductivity due to the monodispersed SiO₂ nanospheres. Huang et al. modified the LLZO by coating dopamine (PDA). The dual wetting capability of dopamine on both inorganic and organic interfaces facilitates the uniform distribution of LLZO in SPEs, leading to homogeneous lithium ion transfer in the composite electrolyte [27]. Another effective way to avoid the filler agglomeration is to fabricate nanostructured 3D fillers, such as SiO₂, LLZO, and LLTO [25, 28–30]. The 3D-filler modified SPEs showed significant enhancement in both ionic conductivity and compatibility with lithium metal anode. Despite these advances, facile synthesis of SPEs with uniformly dispersed ceramic fillers still remains a severe challenge.

Herein, we report a simple spray drying method to avoid agglomeration and increase the mass ratio of fillers for SPEs to adopt polyvinylidene fluoride (PVDF) polymer matrix and garnet Li₄La₃Zr_{1.4}Ta_{0.6}O₁₂ (LLZTO) filler. It should be noted that the PVDF-based SPEs deliver high ionic conductivity with a small amount of solvent, due to the strong chemical interaction between the polymer matrix and the active filler. In addition, compared with the soft PEO with the narrow electrochemical window, the combination of PVDF and LLZTO achieves compatibility with high voltage electrodes [31–33]. The spray drying method is usually used to synthesize materials with core-shell or interconnected structures [34, 35]. Using this method, the PVDF with lithium bis(trifluoromethanesulfonyl)imide (LiTFSI) covers the surface of each LLZTO granules during the nebulization process, which can avoid the filler aggregation during the solvent volatilization process and form a well-arranged organic/inorganic dispersion, therefore ensuring the uniformity of the Young's modulus and surface electric field, further increasing the mechanical strength and establishing orderly arranged lithium-ion transport channels [36, 37]. The as-prepared SPEs present high mechanical strength of 7.1 MPa, high ionic conductivity of 1.86×10^{-4} S·cm⁻¹ at room temperature, and excellent ability for dendrite anti-growth. The LiCoO₂/Li cells assembled with the as-prepared SPEs also display excellent cyclic performance and good rate capability. This study proposes a novel and simple method to avoid the filler aggregation for SPEs, which is an important guidance for the facile and large-scale synthesis of high-performance SPEs.

2 Experiment

2.1 Materials

Dimethyl formamide (DMF), ZrO₂ (99.99%), and Ta₂O₅ (99.99%) were purchased from Aladdin reagent. LiOH (99.995%) and La(OH)₃ (99.95%) were supported by Alfa Aesar reagent. Lithium (bis trifluoromethyl) sulfate (99.95%) and polyvinylidene fluoride were bought from Sigma-Aldrich.

2.2 Preparation of the solid polymer electrolytes

The LLZTO powder was synthesized through a solid reaction, whose detailed description was referred to the previous work [38, 39]. The average size of the LLZTO was 200 nm. The PVDF, LiTFSI, and LLZTO at a weight ratio of 1:0.5:0.2, 0.4 to 1.0 were added into the DMF solvent (500 mL) and dispersed by ball milling. After that, the as-prepared solution was used for preparing the SPEs via spray drying in a N₂ atmosphere (Yamato Spray Dryer ADL311S). The material inlet temperature was controlled at 80 °C and the flow rate of the solution was set at 5

mL·min⁻¹. For comparison, PVDF, LiTFSI, and LLZTO with the same mass ratio were added into the DMF solvent and coated the Teflon plate. We recorded the SPEs prepared by the spray drying method and flow coating method as PVDF/LLZTO-S and PVDF/LLZTO-C, respectively. All the SPEs were stored in a vacuum oven at 80 °C for 24 h to evaporate the solvent, then they were used for the rest experiments. The thickness of the SPEs was 25 ± 2 μm.

2.3 Electrode preparation and cell assembly

The LiCoO₂ (LCO), super-P, and PVDF were mixed at a mass ratio of 80:10:10 for the preparation of cathode. The loading of LCO₂ was set at 3.5–4.0 mg·cm⁻². The lithium metal was used as anode. The cathode/electrolyte interfaces were wetted by 1 μL·cm⁻² ionic liquid (0.1 mol·L⁻¹ LiTFSI dissolved in 1-butyl-1-methylpyrrolidinium bis (trifluoromethylsulfonyl) imide) for better contact.

2.4 Characterization of the electrolytes

The crystal structure of LLZTO was examined via X-ray diffraction (XRD) (Bruker D2 Phaser, Cu Kα radiation in 2θ ranging from 10° to 80°). The morphologies of the SPEs were investigated by a field emission scanning electron microscope (FE-SU4800, Hitachi, Japan). The surface flatness of the membranes, Young's modulus, and surface electric field were characterized by an atomic force microscope (AFM) (PF-KPFM, Bruker, German) with a probe of MESP-V2. The mechanical strength of SPEs was measured by a tensile machine (UTM-4000, SUNS, Shenzhen).

The alternating current (AC) impedance data of electrolytes were measured by an electrochemical workstation (Solartron, SI-1260, England) over a frequency range from 100 kHz to 1 Hz with sandwiching the electrolytes (wetted by 1 μL·cm⁻² ionic liquid) between two stainless electrodes. The measurement was carried out for every 10 °C rise in a temperature range from 90 to 30 °C. Thermogravimetric analysis (TGA) (SDT-650, TA Instruments, Milford, USA) was used to measure the solvent proportion of membrane from 30 to 200 °C at a heating rate of 5 °C·min⁻¹. The electrolytes were clamped between a lithium metal counter electrode and a stainless-steel electrode for the linear sweep voltammetry (LSV) measurement within a voltage range of 0–6 V at 0.5 mV·s⁻¹. X-ray photoelectron spectroscopy (XPS) analysis was characterized by an ESCALAB250 electron spectrometer (Thermo Fisher Scientific, USA).

The Li/LCoO₂ cells with PVDF/LLZTO-S and PVDF/LLZTO-C were charged/discharged between 3.0 and 4.2 V at ambient temperature of 60 °C by the battery test equipment (LAND-V34, Land Electronic, China) to investigate their cyclic and rate performances. The C-rate measurements of Li/LCoO₂ cells were carried out between 3.0 and 4.2 V at varied currents at 60 °C.

3 Result and discussions

3.1 Physical characterizations of SPEs

The LLZTO particles synthesized through solid-state reactions were pulverized by dry ball milling in an Ar atmosphere. The morphology and structure of the as-prepared LLZTO were indicated by scanning electron microscopy (SEM) and XRD measurements respectively. As shown in Fig. S1 in the Electronic Supplementary Material (ESM), the LLZTO presents a pure cubic structure, which is beneficial for high ionic conductivity for SPEs [40, 41]. Figures 1(a)–1(c) display the synthetic route and surface morphology of PVDF/LLZTO-C, presenting the significant agglomeration of the LLZTO particles. According to the previous work, the huge surface energy difference between LLZTO and PVDF solution makes the LLZTO particles tend to aggregate,

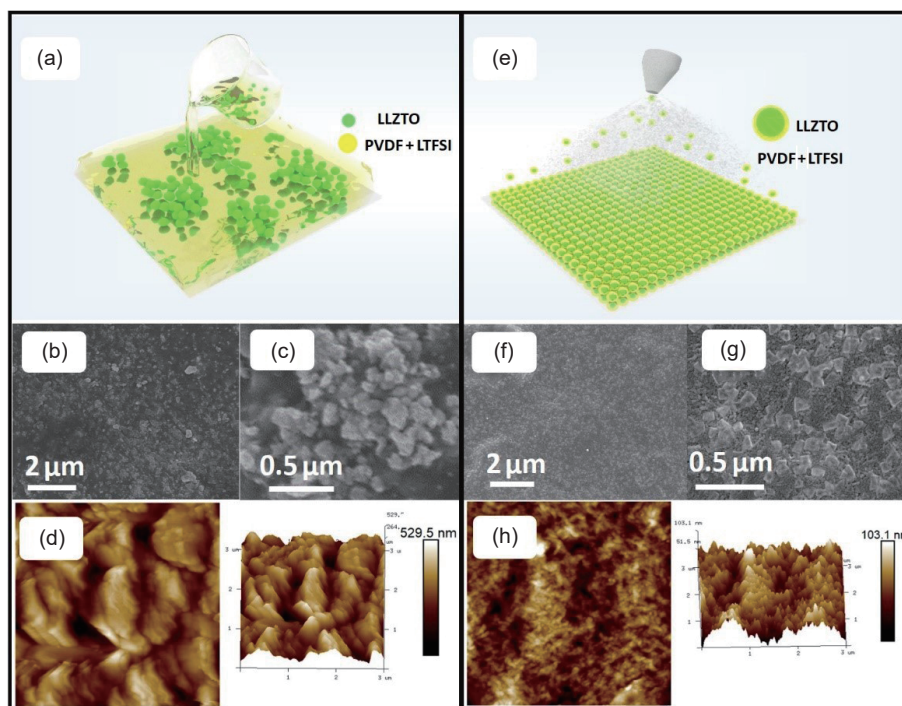


Figure 1 (a) The synthetic route and ((b) and (c)) morphology of SPEs prepared by the flow coating method. Obvious agglomeration of LLZTO particles can be seen. (d) The surface and three-dimensional AFM images of PVDF/LLZTO-C. The scan direction is from bottom to top, and the scan area is $3.0 \mu\text{m} \times 3.0 \mu\text{m}$. (e) The synthetic route and ((f) and (g)) morphology of SPEs prepared via a simple spray drying method. The homogenous dispersion of LLZTO particles can be found. (h) The surface and three-dimensional AFM images of PVDF/LLZTO-S.

especially during the solvent evaporation process. Compared with the PVDF/LLZTO-C membranes, a more homogeneous dispersion of LLZTO particles can be achieved in the PVDF/LLZTO-S membranes, as shown in Figs. 1(e)–1(g). The topography map was confirmed by AFM. As illustrated in Fig. 1(d), the PVDF/LLZTO-C with the LLZTO weight ratio of 35% shows a height above 500 nm, while the PVDF/LLZTO-S presents a much flatter surface at the height of approximately 103.1 nm (Fig. 1(h)). The homogenous dispersion and flat surface are very important for further improvement in mechanical strength and electrochemical performance for SPEs [27, 42].

Mechanical properties of SPEs are of great importance for practical application especially for the assembling process of lithium metal batteries [22]. To evaluate the effect of LLZTO dispersion on the mechanical strength of the SPEs, the Young's modulus dispersion and stress-strain curves of the SPEs were measured. The modulus dispersion is inhomogeneous for the PVDF/LLZTO-C as shown in Fig. 2(a), and the bright area is where the LLZTO agglomeration comes. By contrast, the modulus becomes much more homogeneous for the PVDF/LLZTO-S, as shown in Fig. 2(b), indicating that the PVDF/LLZTO-S has a uniform mechanical field. Consequently, the PVDF/LLZTO-C presents a mechanical strength of 5.2 MPa, while it increases to as high as 7.1 MPa for PVDF/LLZTO-S, as shown in Fig. 2(c). In addition, the local strain % of PVDF/LLZTO-C is reduced due to the agglomeration of LLZTO, resulting in the strain % of PVDF/LLZTO-C approximately 180 is much lower than the 330 for PVDF/LLZTO-S.

3.2 Electrochemical performances

Surface electric field maps of the electrolyte membranes can be obtained through Kelvin probe force microscopy (KPFM), which measures the strength of the electrostatic forces between the membrane and a conductive probe [43–45]. The difference in space charge accumulation on the surfaces of the SPEs results in the dispersion of electric field. The PVDF/LLZTO-S with a potential field of 0–67.5 mV is more uniform than the

PVDF/LLZTO-C with a potential field of 0–333.7 mV, as shown in Figs. 2(d) and 2(e). To evaluate the effect of LLZTO dispersion on the Li^+ conduction, the ionic conductivities (σ_{ion}) were measured. The σ_{ion} of electrolytes is calculated by $\sigma = L/RS$ (R , L , and S are the resistance, thickness, and area of the electrolytes, respectively). The σ_{ion} of SPEs at different weight percent of LLZTO is displayed in Fig. 2(f). The PVDF/LLZTO-S with the LLZTO weight ratio of 35% exhibits a much higher σ_{ion} of $1.25 \times 10^{-4} \text{ S}\cdot\text{cm}^{-1}$ at 30°C than that of PVDF/LLZTO-C with just 12 wt.% LLZTO (the maximum $0.98 \times 10^{-4} \text{ S}\cdot\text{cm}^{-1}$). The electrolytes used in the rest texts are all with the LLZTO weight ratio of 35%. It should be noted that a small amount of bound solvent left in the electrolyte matrix plays an important role in achieving high ionic conductivity for SPEs [46]. Therefore, we measured the weight of the residual solvent with the TGA and displayed the results in Fig. 2(g). The electrolytes suffer less than 10% weight loss below 200°C , which stands for only less than 10% in weight of DMF left for the PVDF/LLZTO-C and PVDF/LLZTO-S. The PVDF/LLZTO-S shows a higher ionic conductivity than the PVDF/LLZTO-C at the same weight ratio of solvent. The above improvement of PVDF/LLZTO-S can be attributed to the high fraction and homogeneous distribution of LLZTO, which provides a high concentration of orderly arranged lithium-ion transfer channels [47]. Figure 2(h) depicts the LSV scans of the electrolytes. An oxidation current at approximately 5.0 V can be seen from the PVDF/LLZTO-S. In the case of PVDF/LLZTO-C, the electrochemical stable window reduces to 4.8 V. It is possibly owing to the heterogeneous surface electric field which leads to the occurrence of some over-potential areas, further resulting in the premature occurrence of local electrolyte decomposition [48]. Besides, compared with the PVDF/LLZTO-C, the PVDF/LLZTO-S has a much flatter surface which can avoid the pitting initiation and development [49].

3.3 Battery performances

From the above analysis, the homogeneous distribution of LLZTO enhances the mechanical strength and ensures the uniformity of

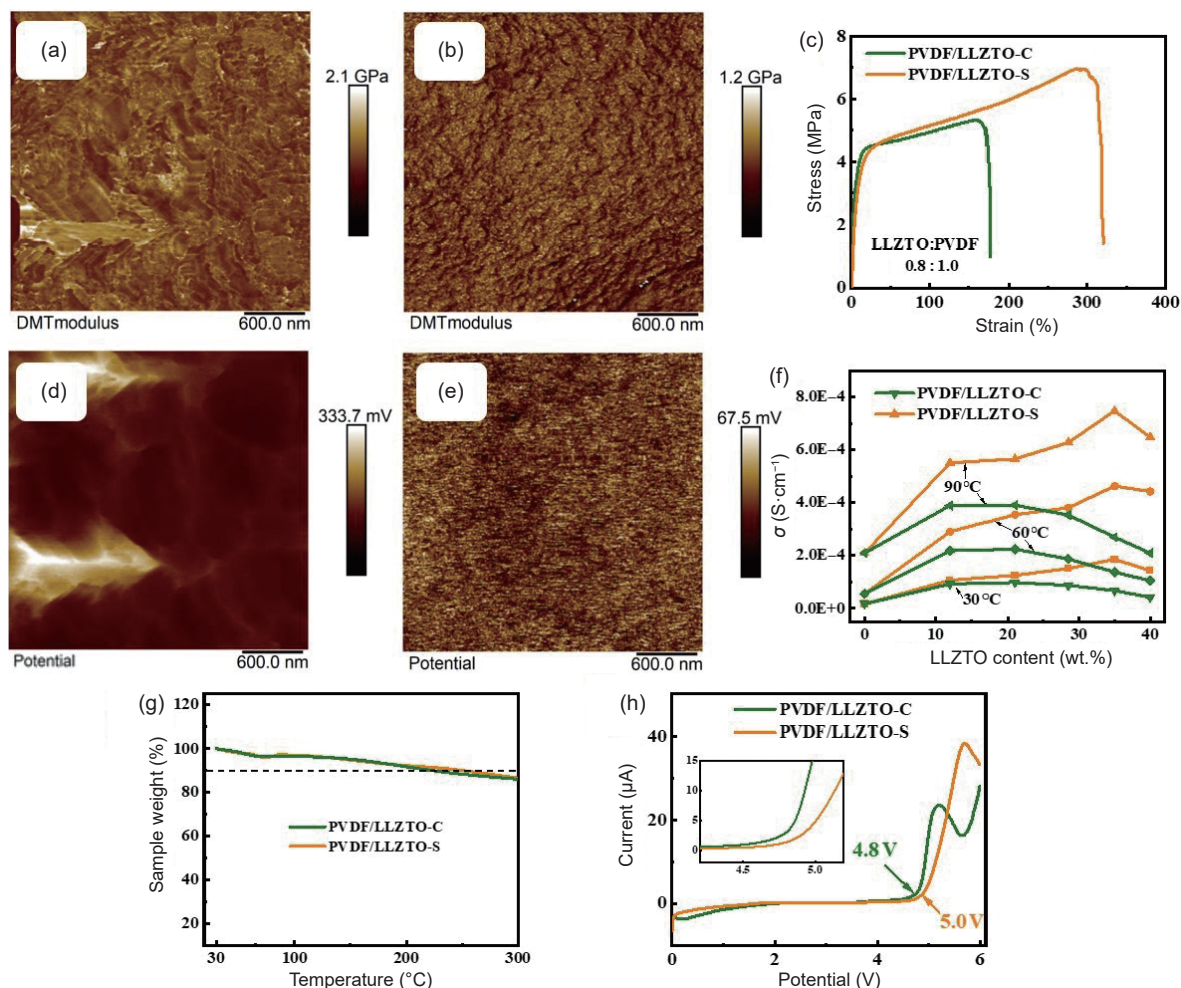


Figure 2 The AFM images of Young's modulus mapping of (a) PVDF/LLZTO-C and (b) PVDF/LLZTO-S. (c) Tensile strength curves of PVDF/LLZTO-C and PVDF/LLZTO-S. The AFM images of surface electric field of (d) PVDF/LLZTO-C and (e) PVDF/LLZTO-S. (f) The ionic conductivity of PVDF/LLZTO-C and PVDF/LLZTO-S at different weight percent of LLZTO at 30, 60, and 90 °C. (g) TGA curves of PVDF/LLZTO-S and PVDF/LLZTO-C. (h) LSV scans at the scanning rate of 1.0 mV·s⁻¹ for the electrolytes.

the electric field, which is critical for the depression of dendrite growth. To demonstrate the compatibility of electrolytes with Li anode, we assembled the Li symmetric cells. As shown in Figs. 3(a) and 3(b), the Li symmetric cells with the PVDF/LLZTO-C electrolytes present significantly increased voltage at a current of 0.1 mA·cm⁻² at 60 °C, but they fail after about 60 h when the voltage increases to the cutoff score (5.0 V) of the battery test equipment (LAND-V34). Using the PVDF/LLZTO-S, the Li symmetric cells exhibit stable cycles over 1,000 h. The interface resistance of the Li symmetric cells before and after Galvanostatic cycling is shown in Figs. 3(c) and 3(d). Compared with the cells assembled with PVDF/LLZTO-C in the significant resistance increasing from 450 Ω to nearly 8.5 kΩ, the cells with PVDF/LLZTO-S present the resistance increasing from 150 to less than 300 Ω. To investigate the effect of the surface electric field on change in the chemical components, the SPEs and Li metal after cycling were detected and analyzed by XPS. Two peaks at 688.6 and 685 eV in the F 1s spectrum for SPEs (Figs. 3(e) and 3(h), and Fig. S2 in the ESM) can be assigned to -CF₃ and LiF, respectively [50]. LiF is mainly originated from the defluorination of the PVDF-HFP electrolyte and degradation of LiTFSI components. The LiF peak of PVDF/LLZTO-C after 50 h is much higher than the PVDF/LLZTO-S after 50 h and on a similar magnitude with PVDF/LLZTO-S after 1,000 h, which indicates PVDF/LLZTO-S shows better electrochemical stability than PVDF/LLZTO-C. To investigate the effect of the surface electric field on the formation of Li dendrite, the cells were disassembled after cycling. As shown

in Figs. 3(f) and 3(i), rough surface with massive Li dendrite is observed on the Li anode for the cells with PVDF/LLZTO-C. In the case of the cells with PVDF/LLZTO-S after cycling for 1,000 h, the surface of solid electrolyte is still smooth and no Li dendrite can be found. This is mainly attributed to the uniform Young's modulus and surface electric field [26, 51, 52]. The schematic illustrations of possible dendrite growth are presented in Figs. 3(g) and 3(j). As reported in the previous work, there are two main possible pathways in the SPEs for the lithium ions, containing polymer matrix and the inorganic electrolytes [5, 37, 47, 53]. The aggregation of LLZTO leads to the uneven plating/stripping of Li⁺ due to the heterogeneous Li⁺ passways and the localized space charge accumulation under the ununiform surface electric field, which easily caused the growth of the dendrite lithium, as shown in Fig. 3(g). As the roots of lithium dendrite are electrically dissolved, some of the lithium dendrites may peel off the electrode, resulting in the formation and accumulation of dead lithium, which increases the polarization potential of the cells. In the case of the electrolytes prepared via the spray drying method, the uniform dispersion of the LLZTO guarantees the homogeneous transport pathways for Li⁺ and the uniform electric field, which avoids the formation of the dendrite lithium, as shown in Fig. 3(i). Besides, the uniform Young's modulus (mechanical hardness) of PVDF/LLZTO-S can prevent lithium dendrite from puncturing the electrolytes in the weak mechanical area of SPEs where lack of LLZTO inorganic fillers.

The charge and discharge curves of Li/LCoO₂ cells with

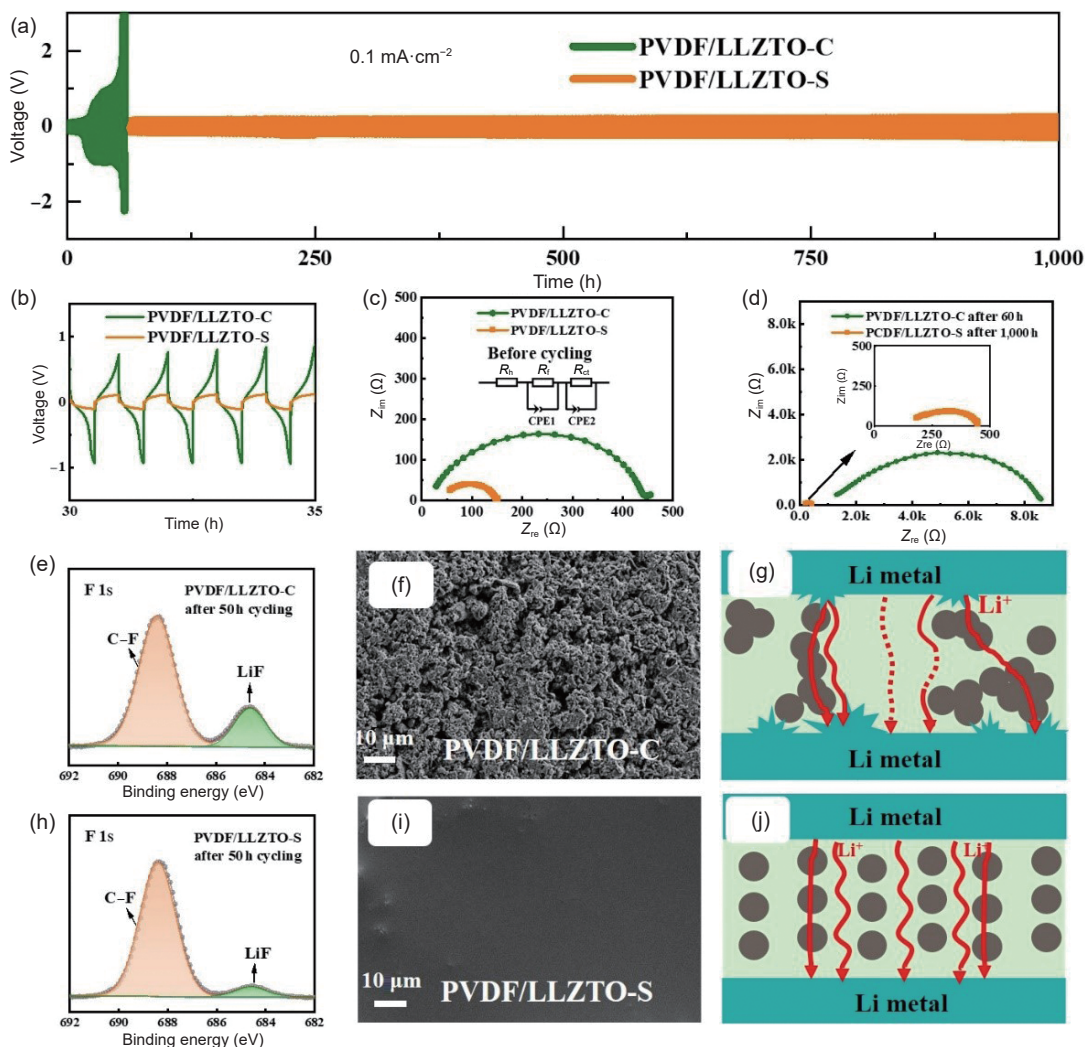


Figure 3 (a) and (b) Galvanostatic cycling profiles of the Li symmetric cells with a current density of $0.1 \text{ mA}\cdot\text{cm}^{-2}$ at 60°C . The Nyquist plots of lithium symmetric cells assembled with PVDF/LLZTO-S and PVDF/LLZTO-C that were measured (c) before and (d) after cycles. The high-resolution XPS spectra of F 1s for (e) PVDF/LLZTO-C and (f) PVDF/LLZTO-S. Typical SEM images of Li metal anodes with (f) PVDF/LLZTO-C and (i) PVDF/LLZTO-S. The schematic illustrations of possible dendrite growth in (g) PVDF/LLZTO-C and (j) PVDF/LLZTO-S.

different electrolytes are given in Fig. 4 and Fig. S2 in the ESM. The cells with PVDF/LLZTO-S present an initialize specific capacity of $140 \text{ mAh}\cdot\text{g}^{-1}$ at 0.2 C rate at 60°C and suffer 14% capacity degradation after 150 cycles. By contrast, only initial $108 \text{ mAh}\cdot\text{g}^{-1}$ and 22 cycles life are exhibited by the cells with PVDF/LLZTO-C (Figs. 4(a) and 4(b)). Furthermore, the cells with PVDF/LLZTO-S maintain a superior Coulomb efficiency of about 99.4% during the cycling. The cells are also charged/discharged at ambient temperature at a charge/discharge rate of 0.5 C. Compared with the tests operated at 60°C , the cells running at room temperature present a slight increase in voltage and deliver an initial specific capacity of $120 \text{ mAh}\cdot\text{g}^{-1}$, as shown in Figs. 4(c) and 4(d). The rate performance of Li/LCoO₂ cells with PVDF/LLZTO-S is shown in Figs. 4(e) and 4(f). The Li/LCoO₂ cells show a gradual increase in ohmic polarization and a decrease in capacity with the increasing current. The specific discharge capacity quickly recovers from 79.3 to $132.3 \text{ mAh}\cdot\text{g}^{-1}$ when the current density returns from 1.0 to 0.1 C, revealing the excellent rate performance of cells with PVDF/LLZTO-S.

4 Conclusion

In summary, a facile and novel spray drying method is used for synthesizing high-performance SPEs. The PVDF with LTFSI covering the surface of each LLZTO granules can not only avoid

the aggregation and increase the fraction of the inorganic fillers, but also guarantee the homogeneous Young's modulus and the surface electric field. Consequently, PVDF/LLZTO-S presents high tensile strength of 7.1 MPa, high ionic conductivity of $1.86 \times 10^{-4} \text{ S}\cdot\text{cm}^{-1}$, and wide electrochemical window up to 5.0 V. The lithium-symmetrical cells show a highly stable Li plating/stripping for over 1,000 h at $0.1 \text{ mA}\cdot\text{cm}^{-2}$. The corresponding Li/LCoO₂ batteries demonstrate good rate capability and excellent cyclic performance with capacity retention of 80% after 100 cycles at ambient temperature. The simple and easy large-scale method provides an important guidance for the synthesis of high-performance SPEs.

Acknowledgements

We gratefully acknowledge the financial support from the National Natural Science Foundation of China (No. 21805147).

Electronic Supplementary Material: Supplementary material (SEM micrographs, XRD scan spectra of LLZTO particles, the high-resolution XPS spectrum of F 1s, and charge/discharge curves of Li|PVDF/LLZTO-C|LCoO₂ at 60°C) is available in the online version of this article at <https://doi.org/10.1007/s12274-021-3683-6>.

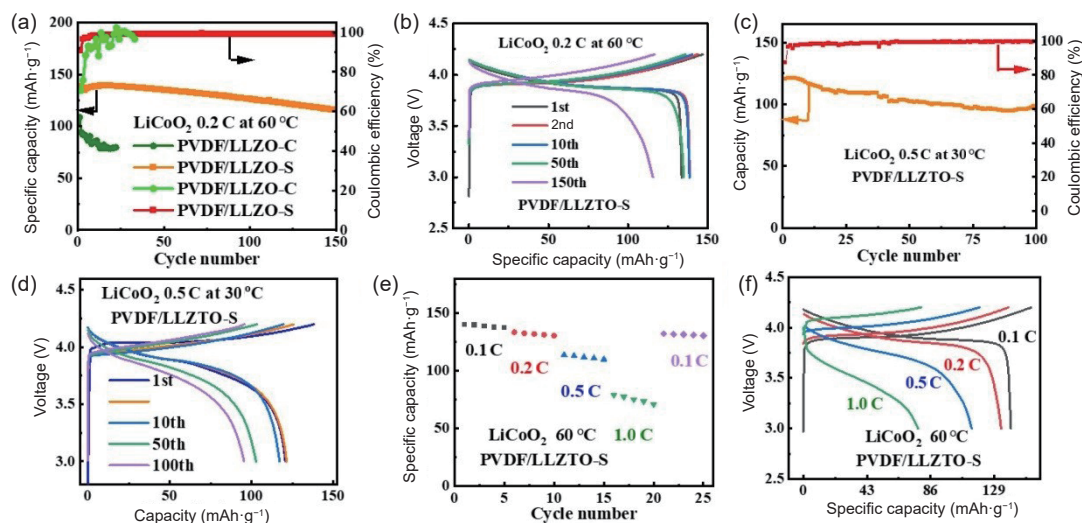


Figure 4 (a) Cycle performance and (b) charge/discharge curves of Li/LiCoO₂ assembled with PVDF/LLZO-S at 60 °C. (c) Cycle performance and (d) charge/discharge curves of Li/LiCoO₂ with PVDF/LLZO-S at ambient temperature. (e) Rate performance and (f) charge/discharge curves of Li/LiCoO₂ with PVDF/LLZO-S at 60 °C.

References

- Cui, J.; Chen, X.; Zhou, Z.; Zuo, M.; Xiao, Y.; Zhao, N.; Shi, C.; Guo, X. Effect of continuous pressures on electrochemical performance of Si anodes. *Mater. Today Energy* **2021**, *20*, 100632.
- Zhang, X. J.; Chen, L. L.; Yang, Z.; Qiu, X. Y.; Zheng, Z. M. Investigation of the structural effect of the carbon coated separator towards to the properties of Li-S batteries. *Mater. Lett.* **2021**, *290*, 129512.
- Yang, Y.; Zhu, H.; Xiao, J. F.; Geng, H. B.; Zhang, Y. F.; Zhao, J. B.; Li, G.; Wang, X. L.; Li, C. C.; Liu, Q. Achieving ultrahigh-rate and high-safety Li⁺ storage based on interconnected tunnel structure in micro-size niobium tungsten oxides. *Adv. Mater.* **2020**, *32*, 1905295.
- Shi, C.; Zhu, J. W.; Shen, X.; Chen, F. X.; Ning, F. G.; Zhang, H. D.; Long, Y. Z.; Ning, X.; Zhao, J. B. Flexible inorganic membranes used as a high thermal safety separator for the lithium-ion battery. *RSC Adv.* **2018**, *8*, 4072–4077.
- Wang, C. W.; Fu, K.; Kammampata, S. P.; McOwen, D. W.; Samson, A. J.; Zhang, L.; Hitz, G. T.; Nolan, A. M.; Wachsman, E. D.; Mo, Y. F. et al. Garnet-type solid-state electrolytes: Materials, interfaces, and batteries. *Chem. Rev.* **2020**, *10*, 4257–4300.
- Manthiram, A.; Yu, X. W.; Wang, S. F. Lithium battery chemistries enabled by solid-state electrolytes. *Nat. Rev. Mater.* **2017**, *2*, 16103.
- Niu, C. J.; Lee, H.; Chen, S. R.; Li, Q. Y.; Du, J.; Xu, W.; Zhang, J. G.; Whittingham, M. S.; Xiao, J.; Liu, J. High-energy lithium metal pouch cells with limited anode swelling and long stable cycles. *Nat. Energy* **2019**, *4*, 551–559.
- Zhou, Q.; Dong, S. M.; Lv, Z. L.; Xu, G. J.; Huang, L.; Wang, Q. L.; Cui, Z. L.; Cui, G. L. A temperature-responsive electrolyte endowing superior safety characteristic of lithium metal batteries. *Adv. Energy Mater.* **2020**, *10*, 1903441.
- Ren, X. C.; Zhang, X. Q.; Xu, R.; Huang, J. Q.; Zhang, Q. Analyzing energy materials by cryogenic electron microscopy. *Adv. Mater.* **2020**, *32*, 1908293.
- Zhang, Q. Q.; Liu, K.; Ding, F.; Liu, X. J. Recent advances in solid polymer electrolytes for lithium batteries. *Nano Res.* **2017**, *10*, 4139–4174.
- Zhang, Z. Z.; Shao, Y. J.; Lotsch, B.; Hu, Y. S.; Li, H.; Janek, J.; Nazar, L. F.; Nan, C. W.; Maier, J.; Armand, M. et al. New horizons for inorganic solid state ion conductors. *Energy Environ. Sci.* **2018**, *11*, 1945–1976.
- Wu, B. B.; Wang, S. Y.; Lochala, J.; Desrochers, D.; Liu, B.; Zhang, W. Q.; Yang, J. H.; Xiao, J. The role of the solid electrolyte interphase layer in preventing Li dendrite growth in solid-state batteries. *Energy Environ. Sci.* **2018**, *11*, 1803–1810.
- Monroe, C.; Newman, J. The impact of elastic deformation on deposition kinetics at lithium/polymer interfaces. *J. Electrochem. Soc.* **2005**, *152*, A396–A404.
- Brissot, C.; Rosso, M. Dendritic growth mechanisms in lithium/polymer cells. *J. Power Sources* **1999**, *81–82*, 925–929.
- Hu, Y. R.; Zhong, Y. R.; Qi, L. M.; Wang, H. L. Inorganic/polymer hybrid layer stabilizing anode/electrolyte interfaces in solid-state Li metal batteries. *Nano Res.* **2020**, *13*, 3230–3234.
- Han, F. D.; Westover, A. S.; Yue, J.; Fan, X. L.; Wang, F.; Chi, M. F.; Leonard, D. N.; Dudney, N. J.; Wang, H.; Wang, C. S. High electronic conductivity as the origin of lithium dendrite formation within solid electrolytes. *Nat. Energy* **2019**, *4*, 187–196.
- Cui, J.; Zhou, Z. H.; Jia, M. Y.; Chen, X.; Shi, C.; Zhao, N.; Guo, X. X. Solid polymer electrolytes with flexible framework of SiO₂ nanofibers for highly safe solid lithium batteries. *Polymers* **2020**, *12*, 1324.
- Lin, D. C.; Liu, W.; Liu, Y. Y.; Lee, H. R.; Hsu, P. C.; Liu, K.; Cui, Y. High ionic conductivity of composite solid polymer electrolyte via in situ synthesis of monodispersed SiO₂ nanospheres in poly(ethylene oxide). *Nano Lett.* **2016**, *16*, 459–465.
- Li, Y.; Zhang, W.; Dou, Q. Q.; Wong, K. W.; Ng, K. M. Li₇La₃Zr₂O₁₂ ceramic nanofiber-incorporated composite polymer electrolytes for lithium metal batteries. *J. Mater. Chem. A* **2019**, *7*, 3391–3398.
- Xie, H.; Yang, C. P.; Fu, K. K.; Yao, Y. G.; Jiang, F.; Hitz, E.; Liu, B. Y.; Wang, S.; Hu, L. B. Flexible, scalable, and highly conductive garnet-polymer solid electrolyte templated by bacterial cellulose. *Adv. Energy Mater.* **2018**, *8*, 1703474.
- Chen, R. J.; Qu, W. J.; Guo, X.; Li, L.; Wu, F. The pursuit of solid-state electrolytes for lithium batteries: From comprehensive insight to emerging horizons. *Mater. Horizons* **2016**, *3*, 487–516.
- Huo, H. Y.; Chen, Y.; Luo, J.; Yang, X. F.; Guo, X. X.; Sun, X. L. Rational design of hierarchical “ceramic-in-polymer” and “polymer-in-ceramic” electrolytes for dendrite-free solid-state batteries. *Adv. Energy Mater.* **2019**, *9*, 1804004.
- Li, Y. T.; Xu, B. Y.; Xu, H. X.; Duan, H. N.; Lü, X. J.; Xin, S.; Zhou, W. D.; Xue, L. G.; Fu, G. T.; Manthiram, A. et al. Hybrid polymer/garnet electrolyte with a small interfacial resistance for lithium-ion batteries. *Angew. Chem., Int. Ed.* **2017**, *56*, 753–756.
- Choi, H.; Kim, H. W.; Ki, J. K.; Lim, Y. J.; Kim, Y.; Ahn, J. H. Nanocomposite quasi-solid-state electrolyte for high-safety lithium batteries. *Nano Res.* **2017**, *10*, 3092–3102.
- Bae, J.; Li, Y. T.; Zhao, F.; Zhou, X. Y.; Ding, Y.; Yu, G. H. Designing 3D nanostructured garnet frameworks for enhancing ionic conductivity and flexibility in composite polymer electrolytes for lithium batteries. *Energy Storage Mater.* **2018**, *15*, 46–52.
- Li, R. G.; Guo, S. T.; Yu, L.; Wang, L. B.; Wu, D. B.; Li, Y. Q.; Hu, X. L. Morphosynthesis of 3D macroporous garnet frameworks and perfusion of polymer-stabilized lithium salts for flexible solid-state

- hybrid electrolytes. *Adv. Mater. Interfaces* **2019**, *6*, 1900200.
- [27] Huang, Z. Y.; Pang, W. Y.; Liang, P.; Jin, Z. H.; Grundish, N.; Li, Y. T.; Wang, C. A. A dopamine modified $\text{Li}_{0.4}\text{La}_3\text{Zr}_{1.4}\text{Ta}_{0.6}\text{O}_{12}$ /PEO solid-state electrolyte: Enhanced thermal and electrochemical properties. *J. Mater. Chem. A* **2019**, *7*, 16425–16436.
- [28] Bae, J.; Li, Y. T.; Zhang, J.; Zhou, X. Y.; Zhao, F.; Shi, Y.; Goodenough, J. B.; Yu, G. H. A 3D nanostructured hydrogel-framework-derived high-performance composite polymer lithium-ion electrolyte. *Angew. Chem., Int. Ed.* **2018**, *57*, 2096–2100.
- [29] Palmer, M. J.; Kalnaus, S.; Dixit, M. B.; Westover, A. S.; Hatzell, K. B.; Dudney, N. J.; Chen, X. C. A three-dimensional interconnected polymer/ceramic composite as a thin film solid electrolyte. *Energy Storage Mater.* **2020**, *26*, 242–249.
- [30] Du, F. M.; Zhao, N.; Fang, R.; Cui, Z. H.; Li, Y. Q.; Guo, X. X. Influence of electronic conducting additives on cycle performance of garnet-based solid lithium batteries. *J. Inorg. Mater.* **2018**, *33*, 462–468.
- [31] Zhang, X.; Liu, T.; Zhang, S. F.; Huang, X.; Xu, B. Q.; Lin, Y. H.; Xu, B.; Li, L. L.; Nan, C. W.; Shen, Y. Synergistic coupling between $\text{Li}_{0.75}\text{La}_3\text{Zr}_{1.75}\text{Ta}_{0.25}\text{O}_{12}$ and poly(vinylidene fluoride) induces high ionic conductivity, mechanical strength, and thermal stability of solid composite electrolytes. *J. Am. Chem. Soc.* **2017**, *139*, 13779–13785.
- [32] Le, H. T. T.; Ngo, D. T.; Kalubarme, R. S.; Cao, G. Z.; Park, C. N.; Park, C. J. Composite gel polymer electrolyte based on poly(vinylidene fluoride-hexafluoropropylene) (PVDF-HFP) with modified aluminum-doped lithium lanthanum titanate (A-LLTO) for high-performance lithium rechargeable batteries. *ACS Appl. Mater. Interfaces* **2016**, *8*, 20710–20719.
- [33] Shi, C.; Dai, J. H.; Huang, S. H.; Li, C.; Shen, X.; Zhang, P.; Wu, D. Z.; Sun, D. H.; Zhao, J. B. A simple method to prepare a polydopamine modified core-shell structure composite separator for application in high-safety lithium-ion batteries. *J. Membrane Sci.* **2016**, *518*, 168–177.
- [34] Leng, J.; Wang, Z. X.; Li, X. H.; Guo, H. J.; Yan, G. C.; Hu, Q. Y.; Peng, W. J.; Wang, J. X. A novel dried plum-like yolk-shell architecture of tin oxide nanodots embedded into a carbon matrix: Ultra-fast assembly and superior lithium storage properties. *J. Mater. Chem. A* **2019**, *7*, 5803–5810.
- [35] Li, Q.; Zhu, G. Z.; Zhao, Y. H.; Pei, K.; Che, R. C. $\text{Ni}_3\text{Mn}_2\text{Co}_2\text{O}$ nanowire/CNT composite microspheres with 3D interconnected conductive network structure via spray-drying method: A high-capacity and long-cycle-life anode material for lithium-ion batteries. *Small* **2019**, *15*, 1900069.
- [36] He, Z. J.; Chen, L.; Zhang, B. C.; Liu, Y. C.; Fan, L. Z. Flexible poly(ethylene carbonate)/garnet composite solid electrolyte reinforced by poly(vinylidene fluoride-hexafluoropropylene) for lithium metal batteries. *J. Power Sources* **2018**, *392*, 232–238.
- [37] Li, Z.; Huang, H. M.; Zhu, J. K.; Wu, J. F.; Yang, H.; Wei, L.; Guo, X. Ionic conduction in composite polymer electrolytes: Case of PEO: Ga-LLZO composites. *ACS Appl. Mater. Interfaces* **2019**, *11*, 784–791.
- [38] Du, F. M.; Zhao, N.; Li, Y. Q.; Chen, C.; Liu, Z. W.; Guo, X. X. All solid state lithium batteries based on lamellar garnet-type ceramic electrolytes. *J. Power Sources* **2015**, *300*, 24–28.
- [39] Li, Y. Q.; Wang, Z.; Li, C. L.; Cao, Y.; Guo, X. X. Densification and ionic-conduction improvement of lithium garnet solid electrolytes by flowing oxygen sintering. *J. Power Sources* **2014**, *248*, 642–646.
- [40] Gao, Z. H.; Sun, H. B.; Fu, L.; Ye, F. L.; Zhang, Y.; Luo, W.; Huang, Y. H. Promises, challenges, and recent progress of inorganic solid-state electrolytes for all-solid-state lithium batteries. *Adv. Mater.* **2018**, *30*, 1705702.
- [41] Thangadurai, V.; Weppner, W. $\text{Li}_6\text{ALa}_2\text{Ta}_2\text{O}_{12}$ (A = Sr, Ba): Novel garnet-like oxides for fast lithium ion conduction. *Adv. Funct. Mater.* **2005**, *15*, 107–112.
- [42] Kim, Y.; Yoo, A.; Schmidt, R.; Sharafi, A.; Lee, H.; Wolfenstine, J.; Sakamoto, J. Electrochemical stability of $\text{Li}_{0.5}\text{La}_3\text{Zr}_{1.5}\text{M}_{0.5}\text{O}_{12}$ (M = Nb or Ta) against metallic lithium. *Front. Energy Res.* **2016**, *4*, 20.
- [43] Burnett, T.; Yakimova, R.; Kazakova, O. Mapping of local electrical properties in epitaxial graphene using electrostatic force microscopy. *Nano Lett.* **2011**, *11*, 2324–2328.
- [44] Panchal, V.; Pearce, R.; Yakimova, R.; Tzalenchuk, A.; Kazakova, O. Standardization of surface potential measurements of graphene domains. *Sci. Rep.* **2013**, *3*, 2597.
- [45] Liu, C.; Li, X.; Revilla, R. I.; Sun, T.; Zhao, J. B.; Zhang, D. W.; Yang, S. F.; Liu, Z. Y.; Cheng, X. Q.; Terryn, H. et al. Towards a better understanding of localised corrosion induced by typical non-metallic inclusions in low-alloy steels. *Corrosion Sci.* **2021**, *179*, 109150.
- [46] Zhang, X.; Wang, S.; Xue, C. J.; Xin, C. Z.; Lin, Y.; Shen, Y. H.; Li, L. L.; Nan, C. W. Response to comment on "self-suppression of lithium dendrite in all-solid-state lithium metal batteries with poly(vinylidene difluoride)-based solid electrolytes". *Adv. Mater.* **2020**, *32*, 2000026.
- [47] Yamada, H.; Bhattacharyya, A. J.; Maier, J. Extremely high silver ionic conductivity in composites of silver halide (AgBr, AgI) and mesoporous alumina. *Adv. Funct. Mater.* **2006**, *16*, 525–530.
- [48] Li, M.; Guo, L. Q.; Qiao, L. J.; Bai, Y. The mechanism of hydrogen-induced pitting corrosion in duplex stainless steel studied by SKPFM. *Corros. Sci.* **2012**, *60*, 76–81.
- [49] Wei, L.; Liu, Y.; Li, Q.; Cheng, Y. F. Effect of roughness on general corrosion and pitting of $(\text{FeCoCrNi})_{0.89}(\text{WC})_{0.11}$ high-entropy alloy composite in 3.5 wt.% NaCl solution. *Corros. Sci.* **2019**, *146*, 44–57.
- [50] Jie, J.; Liu, Y. L.; Cong, L. N.; Zhang, B. H.; Lu, W.; Zhang, X. M.; Liu, J.; Xie, H. M.; Sun, L. Q. High-performance PVDF-HFP based gel polymer electrolyte with a safe solvent in Li metal polymer battery. *J. Energy Chem.* **2020**, *49*, 80–88.
- [51] Tan, S. J.; Zeng, X. X.; Ma, Q.; Wu, X. W.; Guo, Y. G. Recent advancements in polymer-based composite electrolytes for rechargeable lithium batteries. *Electrochem. Energy Rev.* **2018**, *1*, 113–138.
- [52] Zhu, Y. H.; Cao, J.; Chen, H.; Yu, Q. P.; Li, B. H. High electrochemical stability of a 3D cross-linked network PEO@nano- SiO_2 composite polymer electrolyte for lithium metal batteries. *J. Mater. Chem. A* **2019**, *7*, 6832–6839.
- [53] Zheng, J.; Hu, Y. Y. New Insights into the compositional dependence of li-ion transport in polymer-ceramic composite electrolytes. *ACS Appl. Mater. Interfaces* **2018**, *10*, 4113–4120.